

## Numerical support of laboratory experiments: Attenuation and velocity estimations

Erik H. Saenger\* (ETH Zurich), Claudio Madonna (ETH Zurich), Marcel Frehner (ETH Zurich), and Bjarne S. G. Almqvist (ETH Zurich)

### Summary

We show that numerical support of laboratory experiments can significantly increase the understanding and interpretation of the obtained results. First we perform simulations of the Seismic Wave Attenuation Module to measure seismic attenuation of reservoir rocks. Our findings confirm the accuracy of this system. However, precision can be improved by optimizing the sensor positions. Second we model wave propagation for an ultrasonic pulse transmission experiment that is used to determine pressure- and temperature-dependent seismic velocities in the rock. Multiple waves are identified in our computer experiment, including bar waves. The metal jacket that houses the sample assembly needs to be taken into account for a proper estimation of the ultrasonic velocities. This influence is frequency-dependent.

### Introduction

Only in rather simple cases the propagation of elastic waves can be described by exact analytical expressions. Numerical techniques have to be applied for complex geometries, which are usually present in laboratory experimental setups to measure attenuation and ultrasonic velocities. In this paper we consider the influence of the measurement setup on the observed results. We discuss two different experiments performed in the Rock Deformation Lab of the ETH Zurich. However, our findings can also be generalized and applied to similar experiments performed with other instrumental setups for attenuation (O'Connell and Budson, 1977; Spencer, 1981; Batzle et al., 2006), and for ultrasonic velocity measurements (Christensen, 1979; Kern et al., 1999; Kono et al., 2004).

### Numerical Method

For solving the elastodynamic wave equation we use the rotated staggered grid finite-difference technique (Saenger et al., 2000). This method has already been applied at the microscale using digital rock images (Saenger et al., 2011), as well as at the field scale (Steiner and Saenger, 2012). The viscoelastic extension is described in detail in Saenger et al. (2005).

### Simulation of attenuation measurements (2D)

The Seismic Wave Attenuation Module (SWAM) is a module to experimentally measure the seismic attenuation in fluid-bearing rocks (Figure 1). It uses natural rock

samples in an efficient way at in-situ conditions and employs linear variable differential transformers (LVDTs) to measure the bulk strain. The apparatus accurately measures the viscoelastic behavior of rocks at different saturation conditions at low seismic frequencies ( $10^{-2}$ - $10^2$  Hz). The SWAM is designed to operate at a strain below  $10^{-6}$ , where rocks behave linearly, and it allows measuring any kind of rock type independent of their heterogeneity (Madonna et al., 2011).

With our numerical simulations we want to understand the influence of the following experimental specifications on the measured quality factor,  $Q$ :

- (1) instrument design
- (2) position of the displacement sensors
- (3) stiffness of the sample
- (4) confining medium
- (5) interface type sample/module to induce different saturation modes

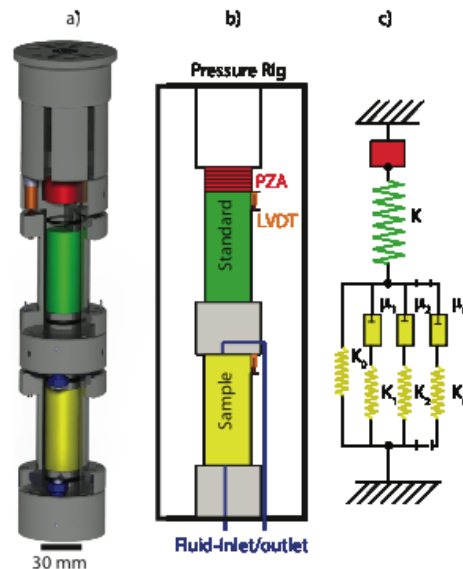


Figure 1. Schematic cross-section of the ETH-developed SWAM. a) CAD drawing, b) Sketched construction, c) Physical model.

For this purpose we created a numerical 2D viscoelastic model of the SWAM (Figure 2). At first glance, this numerical setup is simple and sparsely resolved ( $26 \times 96$  grid points for the regular grid). However, with up to 24 million time steps the viscoelastic simulations take up to 6 hours on a standard laptop.

## Numerical support of laboratory experiments

The 2D model (grid spacing 0.25 cm) consists of a 6.5×25 cm area. The elastic parameters of the different materials are given in Table 1. A sinusoidal vertical displacement source ( $f=[1-10000$  Hz]) is acting on the top while the bottom is fixed. The time step is always  $\Delta t=3.8\times 10^{-7}$  s. This time step is determined by the grid spacing and the maximum elastic moduli in the model. However, for the applied frequencies, this time step is relatively small. The modeling is done with second order time update and with second order spatial differentiation operators.

**Table 1.** Material properties used for the SWAM simulations. The attenuation of the sample (i.e., Plexiglas and rock) is set for the applied excitation frequency to  $Q=12.33$  (Saenger et al., 2005).

Material	Bulk modulus K [GPa]	Shear modulus $\mu$ [GPa]	Density [kg/m <sup>3</sup> ]
Aluminum	114	25	2698
Steel	231.6	77.2	8000
Plexiglas	2.79	1.7	1185
Rock	69.7	23.2	2680

The SWAM uses the sub-resonance method to measure attenuation in the seismic frequency range (Lakes, 2009). For low strain magnitudes ( $\varepsilon < 10^{-6}$ ), which also occur during the propagation of seismic waves, it can be assumed that the rock behaves as a linear time invariant (LTI) system. Hence, the attenuation factor ( $Q^{-1}$ , where  $Q$  is the quality factor) is equal to the tangent of the phase shift between the stress and the strain response signal (Jackson and Paterson, 1987). The sample is cyclically stressed and the phase shift is calculated as the phase difference between the stress and strain signals obtained with the Fast Fourier Transform spectral analysis. Equation 1 shows the relation between the attenuation factor,  $Q^{-1}$ , the phase shift,  $\theta$ , between the stress and strain signals, the energy loss during one cycle,  $\Delta E$ , and the total energy,  $E$ , introduced into the rock while it is deformed (O'Connell and Budiansky, 1977),

$$Q^{-1} = \Delta E / 2\pi E = \tan \theta. \quad (1)$$

In Figure 2 we show some basic input/output of the computer experiment. The distribution of the P-wave modulus,  $M$ , illustrates the input model. During the simulation one can analyze and visualize, for example, the vertical displacement field and the vertical stress field.

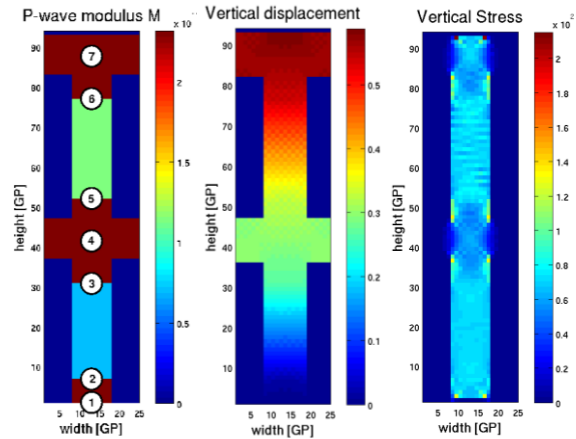


**Figure 2.** Left-hand side: P-wave modulus,  $M$ , of the different parts of the 2D SWAM model. The aluminum reference sample is located between the sensor positions (SP) 5 and 6; the measured sample (rock or Plexiglas) is located between SP 2 and 3. Center: Vertical displacement during a simulation. Right-hand side: The vertical stress is relatively homogeneous in the aluminum, as well as in the rock sample.

To determine which  $Q$ -value is measured by the chosen experimental setup we consider the two possibilities below. The corresponding sensor positions (SP), where the vertical displacement is recorded, are given in Figure 2:

- (1)  $Q_{\text{real}}$ : We analyze the phase shift between [SP4-SP1; phase of applied stress] and [SP7-SP4; phase of strain in the sample]. This is as close to the real experiment as possible. The red solid lines in Figures 3 and 4 correspond to  $Q_{\text{real}}$ .
- (2)  $Q_{\text{opt}}$ : Optimized sensor positions are studied in the second case. The phase shift is analyzed between [SP6-SP5] and [SP3-SP2]. The blue dashed lines in Figures 3 and 4 correspond to  $Q_{\text{opt}}$ .

The main results of our computer experiments are given in Figures 3 and 4 for Plexiglas and rock, respectively. Below, we summarize our main findings:

- (a)  $Q$  can be measured very accurately with the used experimental setup. For frequencies higher or around 100 Hz the results are disturbed by resonance effects of the module.
- (b) The attenuation can be measured more accurately for elastically weaker samples (comparison of  $Q_{\text{real}}(\text{rock})$  vs.  $Q_{\text{real}}(\text{Plexiglas})$ ).
- (c) The SWAM can be improved by repositioning the sensors.  $Q_{\text{opt}}$  is more accurate than  $Q_{\text{real}}$ .
- (d) Additionally, we tested other confining media (e.g., oil) and interface heterogeneities to the sample. These factors do not significantly influence the measurements (not shown here).

## Numerical support of laboratory experiments

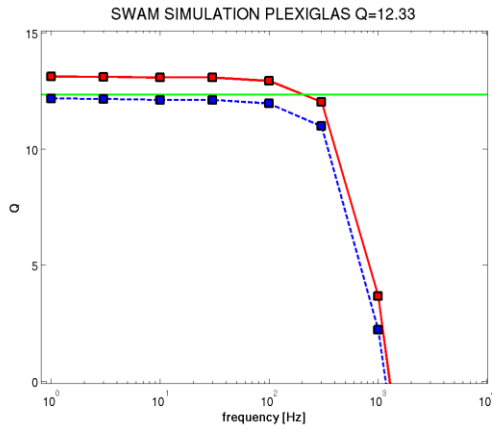


**Figure 3.** Results of the SWAM computer experiments for a Plexiglas sample with an attenuation of  $Q=12.33$  (green line) for a range of applied excitation frequencies.  $Q_{\text{real}}$  (red solid line) can be compared with the real experimental setup. An optimized sensor positioning allow for more accurate measurements of  $Q$  ( $Q_{\text{opt}}$ ; dashed blue line).

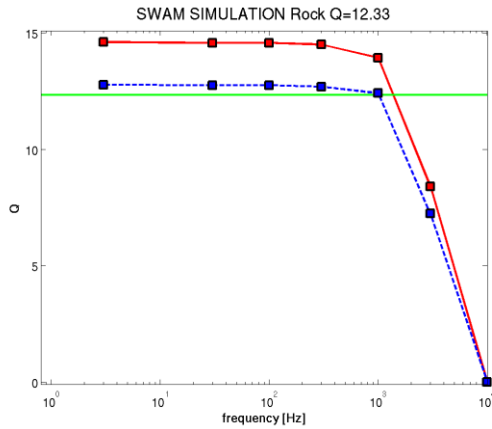


**Figure 4.** SWAM computer experiments, as described in Figure 3, but for the rock sample.

### Simulation of velocity measurements (3D)

Ultrasonic velocity measurements at elevated pressures and temperatures are routinely performed in the laboratory, to investigate rock P- and S-wave velocities at pressure and temperature conditions representing in-situ conditions of the Earth's crust and upper mantle (e.g., Burlini et al., 2005; 2007; Ferri et al., 2007; Caricchi et al., 2008). For this purpose, the internally heated Paterson gas-medium apparatus (Figure 5) is used at the ETH Zurich, with the possibility to reach pressures and temperatures of up to 500 MPa and 1200 °C.

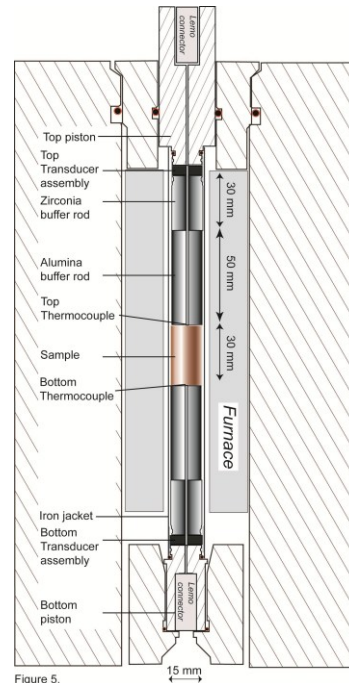


Figure 5.

**Figure 5.** Sample assembly for ultrasonic velocity measurements in the Paterson gas-medium apparatus (redrawn from Burlini et al., 2005). The sample is buffered on each side by aluminum and zirconia rods, which act as thermal insulators protecting the piezoelectric crystals. The assembly is covered by an impermeable iron or copper jacket that prevents the confining medium (argon gas) to enter the sample. The length from top to bottom transducer is 190 mm.

To simulate the ultrasonic experiments of the sample assembly we used a 3D model with  $1275 \times 118 \times 118$  grid points. A cubic elementary cell with an edge length of  $1.5 \times 10^{-4}$  m is chosen. The elastic moduli that were used are summarized in Table 2.

**Table 2.** Used material properties for the ultrasonic simulations.

Material	Bulk modulus K [GPa]	Shear modulus $\mu$ [GPa]	Density [kg/m <sup>3</sup> ]
Alumina	228	152	3890
Zirconia	171	79	6130
Sapphire	307	147	3886
Rock	69.7	23.2	2680
Jacket	166.7	81.5	7874

We have used a body force in vertical direction ( $f=0.1$  MHz or 0.5 MHz) at the top transducer position (Figure 5). The source function is the first derivative of a Gaussian with a time step of  $1.125 \times 10^{-8}$  s. The finite difference algorithm comprises a second order time update and second order space differentiation operators.

## Numerical support of laboratory experiments

As expected, the velocity and amplitude of the waves strongly depend on the frequency of the simulated signal. Even though a relatively simple source-time function is introduced the received signal looks rather complicated due to wave conversion and multiple reflections. It is not straightforward to pick the correct first-arrival times.

It appears that the wave velocity is higher at low frequencies. However, this observation is due to the fact that a part of the energy propagates through the thin metal cover sleeve (jacket), which influences the measured signal at the bottom receiver. This effect is more dominant for waves propagating at 0.1 MHz (red line in Figure 6 vs. red line in Figure 7).

Based on first-arrival time picking in the numerical simulations our best estimate for the velocity of the rock is 5033 m/s at 0.5 MHz (Figure 7), instead of 5100 m/s, which is the correct value we assigned to the rock sample. This would also be estimated in the real experiment.

These observations are important to interpret standard ultrasonic velocity measurements usually performed in the laboratory. Specific numerical experiments, like the ones presented here, are necessary to optimize the velocity determination. The influence of an iron jacket (sometimes required for specific issues) has to be taken into account.

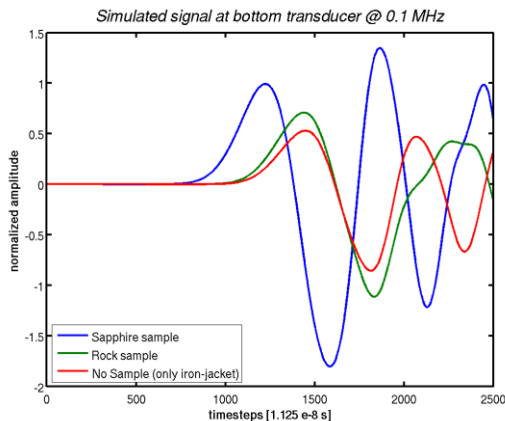


**Figure 6.** Simulated vertical displacement at bottom transducer for the setup shown in Figure 5. The reference signal (blue line) using a Sapphire sample arrives first. The time delay of the signal for the rock sample (green line) is normally used to estimate the velocity of the rock. However, the signal with no sample (red line; wave propagation through the iron jacket only) may disturb the signal for the rock.

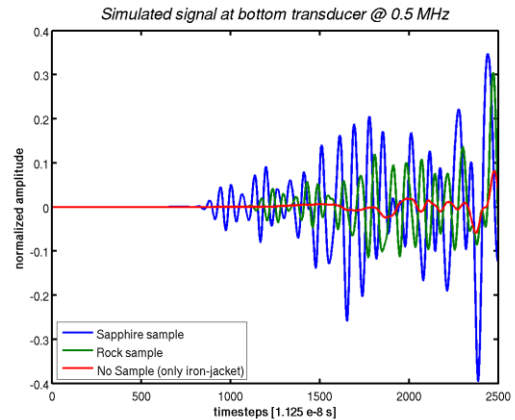


**Figure 7.** Same as Figure 6 but using a source with a fundamental frequency of 0.5 MHz. The influence of the iron jacket is not as strong as for the lower frequency.

## Conclusions

We presented two ongoing numerical studies, which support laboratory investigations. The experimental design can be optimized based on the results of the computer experiments. Simulation of seismic wave propagation on the laboratory scale (somewhere between micro- and field-scale) can help understand and correct findings of real experiments.

For attenuation measurements we suggest an optimized positioning of the sensors. A cut-off frequency has to be determined for similar apparatuses, for which unwanted resonance effects disturb the results. This cut-off frequency also depends on the elastic properties of the considered sample.

For ultrasonic velocity measurements we suggest to take into account the effects of the used jacket and the pieces between the sample and the transducers. All of these experimental pieces have a strong frequency-dependent effect on the recorded signals. Only specific numerical investigations will allow taking them into account.

## Acknowledgments

Our work has been supported by the Swiss Commission for Technology and Innovation (CTI), the Low Frequency Seismic Partnership (LFSP), Spectraseis, and the German Research Foundation (DFG).

#### EDITED REFERENCES

Note: This reference list is a copy-edited version of the reference list submitted by the author. Reference lists for the 2012 SEG Technical Program Expanded Abstracts have been copy edited so that references provided with the online metadata for each paper will achieve a high degree of linking to cited sources that appear on the Web.

#### REFERENCES

- Batzle, M., D. Han, and R. Hofmann, 2006, Fluid mobility and frequency-dependent seismic velocity — Direct measurements: *Geophysics*, **71**, no. 1, N1–N9.
- Burlini, L., L. Arbaret, G. Zeilinger, and J.-P. Burg, 2005, High-temperature and pressure seismic properties of a lower crustal prograde shear zone from the Kohistan arc, Pakistan, *in* D. Bruhn and L. Burlini, eds., *High-strain zones: Structure and physical properties*: Geological Society of London Special Publication 245, 187–202.
- Caricchi, L., L. Burlini, and P. Ulmer, 2008, Propagation of P- and S-waves in magmas with different crystal contents: Insights into the crystallinity of magmatic reservoirs: *Journal of Volcanology and Geothermal Research*, **178**, 740–750.
- Christensen, N. I., 1979, Compressional wave velocities in rocks at high temperatures and pressures, critical thermal gradients, and crustal low-velocity zones: *Journal Geophysical Research*, **84**, 6849–6857.
- Ferri, F., L. Burlini, B. Cesare, and R. Sassi, 2007, Seismic properties of lower crustal xenoliths from El Hoyazo (SE Spain): Experimental evidence up to partial melting: *Earth and Planetary Science Letters*, **253**, 239–253.
- Jackson, I., and M. Paterson, 1987, Shear modulus and internal friction of calcite rocks at seismic frequencies: Pressure, frequency and grain size dependence: *Physics of the Earth and Planetary Interiors*, **45**, 349–367.
- Kern, H., S. Gao, Z. Jin, T. Popp, and S. Jin, 1999, Petrophysical studies on rocks from the Dabie ultrahigh-pressure (UHP) metamorphic belt, central China: Implications for the composition and delamination of the lower crust: *Tectonophysics*, **301**, 191–215.
- Kono, Y., M. Ishikawa, and M. Arima, 2004, Discontinuous change in temperature derivative of  $V_p$  in lower crustal rocks: *Geophysical Research Letters*, doi:10.1029/2004GL020964.
- Lakes, R. S., 2009, *Viscoelastic materials*: Cambridge University Press.
- Madonna, C., N. Tisato, C. Delle Piane, and E. H. Saenger, 2011, Further developments in measurement of low-frequency seismic attenuation in laboratory: 81st Annual International Meeting, SEG, Expanded Abstracts, 2114–2118.
- O’Connell, R. J., and B. Budiansky, 1977, Viscoelastic properties of fluid-saturated cracked solid: *Journal of Geophysical Research*, **82**, 5719–5735.
- Saenger, E. H., F. Enzmann, Y. Keehm, and H. Steeb, 2011, Digital rock physics: Effect of fluid viscosity on effective elastic properties: *Journal of Applied Geophysics*, **74**, 236–241.
- Saenger, E. H., N. Gold, and S. A. Shapiro, 2000, Modeling the propagation of elastic wave using a modified finite-difference grid: *Wave Motion*, **31**, no. 1, 77–92.
- Saenger, E. H., S. A. Shapiro, and Y. Keehm, 2005, Seismic effects of viscous Biot-coupling: Finite difference simulations on micro-scale: *Geophysical Research Letters*, **32**, L14310.

Spencer, J. W., 1981, Stress relaxations at low frequencies in fluid-saturated rocks: Attenuation and modulus dispersion: *Journal of Geophysical Research*, **86**, 1803–1812.

Steiner, B., and E. H. Saenger, 2012, Comparison of 2D and 3D time-reverse imaging — A numerical case study: *Computers and Geosciences*, doi:10.1016/j.cageo.2011.12.005.